Atmos. Chem. Phys., 24, 11807–11822, 2024
https://doi.org/10.5194/acp-24-11807-2024

Atmospheric Chemistry and Physics
Open Access
EGU

Measurement report: In-flight and ground-based measurements of nitrogen oxide emissions from latest-generation jet engines and 100 % sustainable aviation fuel

Theresa Harlass[1], Rebecca Dischl[1,2], Stefan Kaufmann[1], Raphael Märkl[1,2], Daniel Sauer[1], Monika Scheibe[1], Paul Stock[1], Tiziana Bräuer[1,2], Andreas Dörnbrack[1], Anke Roiger[1], Hans Schlager[1], Ulrich Schumann[1], Magdalena Pühl[1], Tobias Schripp[3], Tobias Grein[3], Linda Bondorf[3], Charles Renard[4], Maxime Gauthier[4], Mark Johnson[5], Darren Luff[5], Paul Madden[5], Peter Swann[5], Denise Ahrens[6], Reetu Sallinen[7], and Christiane Voigt[1,2]

[1]Deutsches Zentrum für Luft- und Raumfahrt, Institut für Physik der Atmosphäre, Oberpfaffenhofen, Germany
[2]Johannes Gutenberg-Universität Mainz, Institut für Physik der Atmosphäre, Mainz, Germany
[3]Deutsches Zentrum für Luft- und Raumfahrt, Institut für Verbrennungstechnik, Stuttgart, Germany
[4]Airbus Operations SAS, Toulouse, France
[5]Rolls-Royce plc., Derby, UK
[6]Rolls-Royce Deutschland, Dahlewitz, Germany
[7]Neste Corporation, Innovation, Porvoo, Finland

Correspondence: Tiziana Bräuer (tiziana.braeuer@dlr.de) and Anke Roiger (anke.roiger@dlr.de)

Received: 15 February 2024 – Discussion started: 28 February 2024
Revised: 26 August 2024 – Accepted: 28 August 2024 – Published: 23 October 2024

Abstract. Nitrogen oxides, emitted from air traffic, are of concern due to their impact on climate by changing atmospheric ozone and methane levels. Using the DLR research aircraft *Falcon*, total reactive nitrogen (NO_y) in-flight measurements were carried out at high altitudes to characterize emissions in the fresh aircraft exhaust from the latest-generation Rolls-Royce Trent XWB-84 engine aboard the long-range Airbus A350-941 aircraft during the ECLIF3 (Emission and CLimate Impact of alternative Fuels 3) experiment. The impact of different engine thrust settings, monitored in terms of combustor inlet temperature, pressure and engine fuel flow, was tested for two different fuel types: Jet A-1 and, for the first time, a 100 % sustainable aviation fuel (SAF) under similar atmospheric conditions. In addition, a range of combustor temperatures and an additional blended SAF were tested during ground-based emission measurements. For the data measured during ECLIF3, we confirm that the NO_x emission index increases with increasing combustion temperature, pressure and fuel flow. We find that as expected, the fuel type has no measurable effect on the NO_x emission index. These measurements are used to compare to cruise NO_x emission index estimates from three engine emission prediction methods. Our measurements thus help to understand the ground to cruise correlation of current engine emission prediction methods while serving as input for climate modelling and extending the extremely sparse data set on in-flight aircraft nitrogen oxide emissions to newer engine generations.

Published by Copernicus Publications on behalf of the European Geosciences Union.

1 Introduction

Aviation is a steadily growing transport sector (Lee et al., 2021), even despite the short-term drop during the COVID-19 pandemic (Le Quéré et al., 2020; Schumann et al., 2021; Voigt et al., 2022). As a result, emissions from air traffic are also expected to increase continuously, and higher aircraft and engine efficiencies are surpassed by the overall air traffic growth. The exhaust of an aircraft engine burning conventional kerosene is constituted of ~ 3.16 kg carbon dioxide (CO_2) and ~ 1.23 kg water vapour (H_2O) per kg of fuel burned (Lee et al., 2021) on average. Further emissions depend on the engine type, power settings, combustor technology and fuel composition and include nitrogen oxides (NO_x) as the sum of nitric oxide (NO) and nitrogen dioxide (NO_2), carbon monoxide (CO), unburnt hydrocarbons (C_xH_y), sulfur dioxide (SO_2), and soot (or non-volatile particulate matter, nvPM).

Most recent estimates (Lee et al., 2021) state that aviation since its historical beginnings has been contributing to about 4 % to 5 % of total anthropogenic effective radiative forcing (ERF) with $+100.9$ (55–145) mW m^{-2} (Grewe et al., 2019; Lee et al., 2021). Thus, air traffic emissions have a warming effect on climate. Contrail cirrus clouds hereby represent the largest share of aviation ERF with ~ 57 %, followed by CO_2 (~ 34 %) and NO_x emissions (~ 17 %; Lee et al., 2021). NO_x emissions from aviation contribute indirectly to anthropogenic ERF via a short-term warming and a long-term cooling effect (Brasseur et al., 1996; IPCC, 1999, 2001; Köhler et al., 2008; Lee et al., 2010, 2021; Dahlmann et al., 2011; Grewe et al., 2019; Skowron et al., 2021; Terrenoire et al., 2022). The net ERF from NO_x, in sum, is however positive with 17.5 (0.6–29) mW m^{-2} (Lee et al., 2021). Other studies indicate that the contribution of NO_x in aviation ERF may be even higher due to simplifications in the methodology of previous estimates (Grewe et al., 2019). In the future, aviation NO_x emissions may have a net negative ERF, as the effect of emission of aircraft NO_x depends strongly on background emissions (Skowron et al., 2021).

Up to now, there has been a lack of experimental measurements of NO_x emissions at cruise altitudes from state-of-the-art jet engines. Thus, in the joint Emission and CLimate Impact of alternative Fuels 3 (ECLIF3) project, direct (NO_x, CO, nvPM, H_2O) and indirect aircraft emissions (ice particles, vPM) were measured at high altitudes to understand and assess the impact of modern air traffic on the atmosphere; see also Märkl et al. (2023) and previous related projects such as in Voigt et al. (2021). In this study, we present a comprehensive set of NO_y emission measurements performed in the exhaust of the Airbus A350-941 with Rolls-Royce Trent XWB-84 engines. We derive emission indices from in-flight measurements and compare them to ground-based measurements and three different engine emission prediction methods. We further investigate the effect of the Airbus aircraft burning 100 % sustainable aviation fuel (SAF). Replacing conventional kerosene with SAF is one promising approach to reduce engine soot emissions, ice crystal number concentrations in contrails and the related climate impact, all in addition to a potential reduction of the CO_2 footprint in the life cycle analysis (Voigt et al., 2011, 2021; Moore et al., 2017; Kleine et al., 2018; Bräuer et al., 2021b, 2021a).

2 Materials and methods

2.1 In-flight NO_y and CO_2 measurement methods during ECLIF3

The DLR-operated research aircraft *Falcon* (reg. D-CMET, *Dassault Falcon* 20-E5), a twin-engine jet, was used as the airborne measurement platform. The in-flight instrumentation consisted of several cabin-mounted trace gas (NO_y, CO, CO_2, H_2O) and aerosol instruments with their sample inlets located on the upper fuselage; see Fig. 1b. Also, cloud particle probes were mounted on underwing pods to measure ice particle number concentrations and size distributions in ambient conditions (Märkl et al., 2023). Here, we focus on the NO_y and CO_2 measurement instruments as they are needed to derive the respective NO_x emission indices (EI(NO_x)).

A well-established technique for measuring reactive nitrogen species, as employed in the present paper, includes their catalytic conversion to NO and subsequent detection using chemiluminescence technique (ICAO, 2017). In general, chemiluminescence detectors (CLDs) are widely used in atmospheric monitoring because they are sensitive with a detection limit as low as a few parts per trillion (ppt). In the CLD, a sample of air passes through a reactor where NO is excited to NO_2^* by the reaction with high concentrations of O_3 produced by an ozone generator (Ridley and Howlett, 1974; Drummond et al., 1985). When the excited NO_2^* molecules return to their ground state, the light emitted by the chemiluminescence reaction is proportional to the concentration of NO in the sample. Using selective converters directly upstream of the measurement chamber, different reactive nitrogen species are converted to NO and subsequently detected by the CLD (Bollinger et al., 1983; Fahey et al., 1985). Within DLR, different types of CLDs have been used for atmospheric background measurements (Schlager et al., 1997; Ziereis et al., 2000, 2022; Schmitt, 2003; Stratmann et al., 2016) as well as in-plume detections (Schulte and Schlager, 1996; Schlager et al., 1997; Roiger et al., 2015). Aboard the *Falcon* a heated gold converter ($T = 290$ °C) with hydrogen (H_2) as a reducing agent catalytically reduces all NO_y compounds to NO. NO_y is the sum of NO_x (NO and NO_2) and all other reactive nitrogen species, for example nitric acid and peroxyacetylnitrate (PAN). The instrument offers no measurement of NO_x or the NO_x / NO_y ratio. The time resolution of the instrument is ~ 1 Hz with a detection limit of ~ 0.5 ppb. Under normal operating conditions, the detector runs into saturation-above-mixing ratios of ~ 1000 ppb or $\sim 1 \times 10^6$ counts per second. In or-

der to measure at higher concentrations as expected in the exhaust plumes, a dilution system was integrated supplying zero air to the sample air at a ratio of 1 : 1 prior to the measurement. The NO_y measurement accuracy ranges between ∼ 5 ppb near the detection limit and ∼ 490 ppb at the highest detected mixing ratios of ∼ 4 ppm. It includes the following uncertainty parameters typical for CLD instruments (for details, see Stratmann, 2013): the sensitivity of the instrument (841 ± 95 counts per part per billion, ppb), the efficiency of the NO_y converter (98.7 ± 1.5 % at low and ±30 % at high concentrations), the instrumental interferences due to desorption processes and dark current (36 ± 118 counts), the statistical uncertainty of count rates (150–1600 counts), the uncertainty in the calibration standard (1 % as stated by the manufacturer), and the uncertainty due to the dilution system (7 %–21 %) and due to a second instrument stage above 1×10^6 counts s^{-1} (i.e. 300 ppb).

A high frequency (∼ 10 Hz) non-dispersive infrared gas analyser (LI-7000, LI-COR Biosciences) was used aboard the *Falcon* for in-plume CO_2 detections to be able to capture the small-scale variability of the plume. The LI-7000, uniquely modified in-house for aircraft deployment, uses two measurement chambers to detect CO_2: one is constantly flushed with dry zero air, and the other is supplied with ambient air. The difference in absorption of infrared radiation passing through both cells is used to determine the absolute absorption and the absolute CO_2 mixing ratio (LI-COR, 2007). In the post-processing, the CO_2 mixing ratio is corrected for dilution effects (LI-COR, 2003) and reported as the dry-air mole fraction. The CO_2 accuracy of the LI-7000 is independent with respect to the measured mixing ratios and is around 0.2 ppm. This includes the reproducibility of the calibration standards (0.08 ppm), the precision (0.08 ppm) and the uncertainty of water vapour measurement and thus the dilution correction (0.16 ppm). An occurring trend of the instrument response with instrument temperature and time is compensated for by frequent zero measurements every 30 min during the flight. Absolute CO_2 mixing ratios and background values were cross-checked with a second instrument aboard the *Falcon*, a cavity ring-down spectrometer (CRDS; Picarro G2401-m), due to its stable instrument performance (Fiehn et al., 2020; Klausner et al., 2020; Klausner, 2020).

2.2 In-flight emission sampling strategy

In-flight measurements at high altitudes were carried out under the framework of ECLIF3 in April 2021 (referred to as ECLIF3-1) and in November 2021 (referred to as ECLIF3-2). This joint project was led by DLR and Airbus with Rolls-Royce, Neste, the University of Manchester and the National Research Council Canada (NRC) as partners. The objective of these flight experiments was to characterize emissions behind an Airbus A350-941 (reg. F-WXWB) with Rolls-Royce Trent XWB-84 engines (ECLIF3-1: engine number 21004,

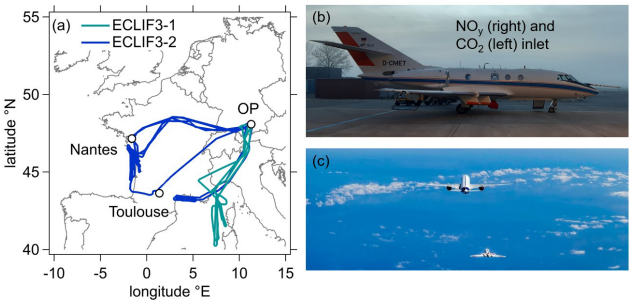

Figure 1. **(a)** Map of the *Falcon* flight routes, **(b)** inlet positions for trace gas sampling aboard the *Falcon* and **(c)** *Falcon* aircraft catching up to the Airbus A350 to perform emission measurements. ©Airbus 2021. Photo by Sylvain Ramadier.

ECLIF3-2: engine number 21012). This twin-engine aircraft is used for long-range distances by many operators since it is more fuel-efficient than a four-engine long-range aircraft and older two-engine aircraft. During the mission flights, the Airbus aircraft was able to feed the engines from separate fuel tanks. Hence, measurements with two different fuels could be performed within single measurement flights, which allowed probing of emissions at similar atmospheric conditions. As a reference fuel, conventional Jet A-1 was used and provided by the local fuel supplier TotalEnergies. As sustainable aviation fuel, a 100 % HEFA-SPK (hydroprocessed esters and fatty acids–synthetic paraffinic kerosene) made from sustainably sourced renewable waste and residues such as used cooking oil and other waste fat was provided by the project partner Neste.

Emission measurements in the near field were performed as closely as possible to the Airbus aircraft at distances between 65 and 470 m (mean of 260 m), resulting in young plume ages of 0.3 to 3.5 s (mean of 0.8 s) in order to sample the fresh emissions before they undergo chemical processing in the atmosphere. Furthermore, it was aimed to study the emissions for various fuels at different combustor inlet parameters (temperature T3, pressure P3, engine fuel flow or fuel-to-air ratio) by varying the engine power settings and flight altitudes in defined but variable test point sequences. In total, six emission chase flights were performed along the western and southern French coast in temporary reserved air space, as shown in Fig. 1a. The *Falcon* was mainly based in Oberpfaffenhofen (OP), Germany, and for a 5 d period in Toulouse, France, to minimize transfer flight times to the Airbus test area. With a takeoff from OP, the *Falcon* had to be refuelled in Nantes prior to the measurement flights along the Atlantic coast.

An example of an emission time series is shown in Fig. 2. Measurements took place in the near field with the *Falcon* aircraft flying behind the Airbus aircraft under non-contrail-formation or only short-lived contrail-formation conditions. Usually, emissions were sampled from the right-hand-side engine, which was operated at different, well-defined cruise

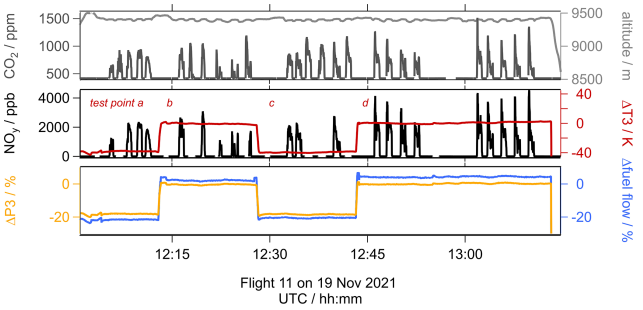

Figure 2. Emission measurement sampling sequence during the flight on 19 November 2021. Trace gases (CO_2, NO_y) and flight altitude as measured aboard the *Falcon*. Change in Airbus aircraft engine parameters (delta fuel flow, delta T3 temperature, delta P3 pressure) indicates different engine test points.

combustor inlet temperature conditions. The *Falcon* is the slower-flying aircraft, with a maximum cruise speed of $\sim 200\,\mathrm{m\,s^{-1}}$. To ensure that both aircraft speeds match in order to maintain the close distance, the Airbus aircraft had to adjust its speed by operating the left engine at a lower thrust. Hence, the test conditions probed in this study are not fully representative of typical cruise conditions. In addition, the Airbus aircraft also typically flies at higher altitudes (above FL350) compared to the altitudes that were sampled within this project (FL180 to 360). Generally speaking, this means that, at fixed T3 and DISA (Delta International Standard Atmosphere), the EI(NO_x) measured at the lower test altitudes tends to be higher than the actual EI(NO_x) at typical cruise altitudes (due to higher P3 at lower altitudes). Nevertheless, we assume that above FL300, this effect is small, and the measurements can be directly compared to predictions at test conditions.

To ensure that the ceiling with the trace gas inlets is directly located in the exhaust plumes, the *Falcon* approached the exhaust trail from slightly lower altitudes. This position was held for ~ 50 s, and then the *Falcon* dropped down to measure atmospheric background conditions for ~ 30 s. This alternating sequence was repeated three to five times for each test point with fixed engine parameters. Large enhancements (Δ) of CO_2 and NO_y were clearly visible with values typically between 100–800 ppm (ΔCO_2) and 500–4000 ppb (ΔNO_y) above mean atmospheric background values of 414–419 ppm and 0.6–4 ppb, respectively.

In Sect. 3.3, we will use additional in-flight far-field measurements from ECLIF3 for a comparison with engine emission prediction methods to achieve more representative cruise conditions. Far-field measurements hereby represent measurements at distances between 6 and 38 km (mean of 20 km) in the aged exhaust (30 to 390 s). Representative cruise conditions aim at similar Mach numbers which can only be achieved when the Airbus is flying at its typical speed.

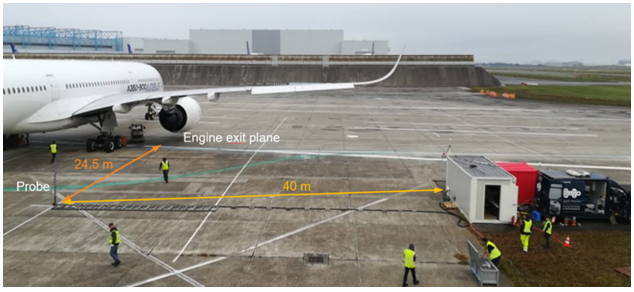

Figure 3. Setup of ECLIF3-2 ground-based measurements behind the A350 with the stainless steel probe and heated stainless steel line. White container: particle measurement instruments for analysing particulate matter in the exhaust. Red container: location of the proton transfer reaction mass spectrometer (PTRMS) for the detection and quantification of volatile organic compounds (VOCs). Blue mobile laboratory: measurement devices for gaseous species, including instruments for measuring NO_y and CO_2.

2.3 Ground-based NO_y and CO_2 measurement methods during ECLIF3-2

In-flight measurements during ECLIF3-2 are complemented by ground-based measurements of the same engine performed in Toulouse, France, in October 2021. The CO_2 concentration was monitored using two non-dispersive infrared (NDIR) sensors (LI-7200RS and LI-850 by LI-COR Biosciences). The NO_y concentration was monitored using two chemiluminescence detectors (CLD 64 and CLD 700 by ECO PHYSICS), which use converters operated at 400 °C. The instruments were calibrated with certified calibration gases before each ground-based test run. Figure 3 shows the measurement setup for the ground-based measurements. Sampling was performed with a stainless-steel probe inlet at a height of 2.6 m and a distance of 24.5 m to the right-hand-side engine exit plane. The exhaust was transported from the probe inlet via a 40 m heated stainless-steel line to a manifold that allowed even distribution of air to the different measuring instruments.

During the ground-based measurements, three fuel types were tested (see Table 1). The measurements with fossil Jet A-1 were performed on 22 October 2021 (ambient temperature: 12.2–14.4 °C; ambient relative humidity: 87 %–81 % during test run). The neat HEFA-SPK and an additional fuel blend (HEFA-SPK blended with a different Jet A-1) were tested on 23 October 2021 (ambient temperature: 9.1–15.2 °C; ambient relative humidity: 47 %–96 % during test run). Four test points with Jet A-1 were measured on both days to identify any biases from changes in ambient conditions or different probe alignment.

The test grid of the ground-based measurements consisted of varied T3 temperatures for the combustor stage settings, ranging from idle to maximum power. Each test point was stabilized for a few minutes, and after reaching a stable T3, sampling was performed for 5–6 min. In the case of the high-

est thrust settings, the sampling time was reduced to 2–3 min. The sampling height and distance were chosen to ensure representative capture of the exhaust plume, while the heated line helped prevent condensation and potential losses or alterations in the sample composition. The use of various measuring instruments and redundant systems further enhanced the accuracy and reliability of the data collected. The different gains of the chemiluminescence detectors allowed for precise measurement of a wide range of NO_y concentrations, while the multiple measuring points of the NDIR systems ensured continuous monitoring of CO_2 concentrations. The selection of T3 temperatures and the varying operational conditions of the combustor stages from idle to maximum power allowed for a comprehensive analysis of emissions under different operating conditions.

2.4 Emission index calculation and plume definition

In order to quantify exhaust emissions from aircraft, the most common metric is the so-called emission index (EI), i.e. an emission quantity per mass of burned fuel. The NO_x emissions index ($EI(NO_x)$) is defined by convention in mass units of NO_2 (Voigt et al., 2012; ICAO, 2017, 2023); hence the sum of NO and NO_2 in ambient air is calculated as if all NO were in the form of NO_2. Several studies discuss the composition of the different nitrogen species in the engine exhaust; for example, Kärcher et al. (1996), Tremmel et al. (1998), Bradshaw et al. (2000), Wormhoudt et al. (2007) and Voigt et al. (2012) agree that at high engine power settings, NO_x in the exhaust is dominated by NO (> 80 %). With growing plume age, the $NO : NO_2$ ratio is determined by an equilibrium of the reaction of NO and O_3, forming NO_2, and the photolysis of NO_2 (Tremmel et al., 1998). In addition, small amounts of HNO_2, HNO_3 and HONO are formed in the ageing plume from the NO_x emissions (Jurkat et al., 2011; Lee at al., 2011). During ECLIF3, only NO_y and no NO_x concentrations were measured aboard the *Falcon*. NO_x concentrations are expected to be close to NO_y, and the fraction of nitrogen acids in the exhaust gas is assumed to be smaller than the NO_y mean measurement accuracy. Hence, all reactive nitrogen species in the exhaust are detected and related to the initial NO_x emissions. For each individual plume encounter, $EI(NO_x)$ is derived based on the inert dilution tracer CO_2 via Eq. (1) following Schulte et al. (1997):

$$\mathrm{EI}(\mathrm{NO}_x) = \frac{\int \Delta \mathrm{NO}_y}{\int \Delta \mathrm{CO}_2} \cdot \mathrm{EI}(\mathrm{CO}_2) \cdot \frac{M(\mathrm{NO}_2)}{M(\mathrm{CO}_2)}, \tag{1}$$

where $\int \Delta NO_y$ and $\int \Delta CO_2$ are the integrated enhancement above an atmospheric background level, $EI(CO_2)$ is the emission index of CO_2 dependent on the fuel used (see Table 1), and $M(NO_2)$ and $M(CO_2)$ are the molar masses of NO_2 (46.0055 g mol^{-1}) and CO_2 (44.0095 g mol^{-1}).

An individual in-flight plume encounter denotes a plume crossing in a time series where enhancements of NO_y and CO_2 start exceeding background level variations, denoting the plume beginning, and the subsequent return to atmospheric background level, denoting the plume end. Between plume beginning and end, a minimum 7 s plume length threshold was chosen to exclude accidental plume encounters. Further, plumes were rejected due to Airbus aircraft engine instability (e.g. variability of T3 greater than ±2 K) and/or low correlation between CO_2 and NO_y measurements ($R < 0.7$). The individual plume crossings of the background-corrected mixing ratios of each species are integrated over time (and, hence, over the horizontal extent of the plume) to account for the inlet positions (about 30 cm difference in the horizontal direction), tubing lengths and different instrument response times. Due to the variable position of the *Falcon* aircraft within the turbulent exhaust plume and thus variable plume dilution values, it is necessary to normalize NO_y mixing ratios to the measured CO_2 concentration. CO_2 hereby acts as a chemically inert species to determine the dilution of the engine emissions at the measurement point. CO_2 emission indices are a fuel-dependent metric and are derived from the hydrogen content and carbon content of the fuel under the assumption that they are completely burnt and all available carbon is converted to CO_2. The emission index $EI(CO_2)$ can then be calculated via Eq. (2) following Moore et al. (2017):

$$\mathrm{EI}(\mathrm{CO}_2) = \frac{\mathrm{RT}}{pV_\mathrm{m}} \cdot \frac{M(\mathrm{CO}_2)}{M(\mathrm{C}) + \alpha M(H)}, \tag{2}$$

where R is the ideal gas constant (8.31 J mol^{-1} K^{-1}), T and p are the temperature (273.15 K) and pressure (101 325 Pa) at standard conditions, V_m is the molar volume at standard conditions (0.0224 m^3 mol^{-1}), $M(C)$ and $M(H)$ are the molar masses of carbon (12.01 g mol^{-1}) and hydrogen (1.01 g mol^{-1}), and α is the hydrogen-to-carbon molar ratio of the fuel (as calculated based on Table 1). As the batches of the fuel supplier varied between the two measurement experiments, the fuel properties also slightly varied. Their characteristic hydrogen and carbon contents are listed in Table 1 together with the calculated emission index of CO_2. The aromatics content was partly determined by GC × GC (mass-based) measurements due to the contents being below the ASTM D6379 (volume-based) detection limits. Samples were taken at different points of the fuelling process. The hydrogen content was measured via low-resolution nuclear magnetic resonance spectrometry (ASTM D3701 with a repeatability of 0.09 % and reproducibility of 0.11 %). The carbon content is assumed to add up to 100 mass percent (hereafter mass %) with the hydrogen content and sulfur content (not listed) and was cross-checked via ASTM D5291 (which has a repeatability of 0.94 % and reproducibility of 2.42 %). The energy content of the fuels does not differ significantly.

2.5 Ground-based ICAO Aircraft Engine Emissions Databank

The reporting of emissions in the vicinity of airports is mandatory for engine manufacturers during certification processes for individual engine types, and reports are voluntarily made publicly available at the International Civil Aviation Organization (ICAO) Aircraft Engine Emissions Databank. For that, a landing-and-takeoff (LTO) cycle is defined to derive emissions during taxi-out/taxi-in, approach, climb and takeoff in a consistent manner (ICAO, 2017). While varying the engine power settings, and thus the fuel flow rate at a test stand, emissions at sea level conditions are measured. Thrust levels of 7 %, 30 %, 85 % and 100 % hereby correspond to taxi-in/taxi-out, approach, climb and takeoff conditions.

As NO_x emissions highly depend on temperature and pressure in the engine combustor, they are derived for different thrust settings related to different flight phases at certification ground test for International Standard Atmosphere (ISA) conditions. In general, NO_x emissions increase with increasing power and increasing fuel flow; see Fig. 4. Thermal NO formation, first described by Zeldovich in 1946 and therefore also referred to as the Zeldovich mechanism, is one of the main sources of nitrogen oxides in combustion, dominating at high pressure and temperature conditions typical for a jet engine (Lavoie et al., 1970). However, as chemical equilibrium of the thermal NO formation route is not reached within typical timescales of a combustor, total formed NO_x in a modern rich burn combustor is strongly dependent on the quick quenching and mixing of the hot streams of the primary combustion zone. The combustor design optimized for NO_x emissions aims to enhance mixing and reduce residence time in areas of high temperature. For a given combustor design, NO_x emissions depend on operating conditions as pressure, temperature and local air-to-fuel ratio in the combustor. NO_x in a gas turbine combustor, i.e. at high pressure and temperature, is predominantly formed via thermal NO pathway. Thermal NO_x formation rate increases exponentially with temperature and further depends on pressure (Gokulakrishnan and Klassen, 2013). In comparison to all $\sim$560 engine types covered by the ICAO Aircraft Engine Emissions Databank (depicted in greyish/black; (EEDB, 2021)), NO_x emissions from the Rolls-Royce Trent XWB-84 engine (depicted in blue) are rather at the upper limit when considering the thrust settings but typical for a modern large engine powering the long range planes. This engine is specifically designed for a modern long-range aircraft being the most fuel-efficient large aero-engine in revenue service, and therefore it operates at high pressure ratios and combustor exit temperatures to deliver the required thrust at high fuel efficiency. Therefore, NO_x emissions tend to be higher than for engines operating at lower overall pressure ratio (OPR).

The certification engine emission data cover a standardized LTO cycle intended to cover local air quality. To predict EIs of the whole flight envelope, different modelling

Table 1. Fuel properties during the measurement experiments. EI(CO_2) is estimated following Moore et al. (2017). The last column denotes the test points used for EI(NO_x) calculation.

	Method	Fuel type	Density at 30 °C (g cm^{-3})	Aromatics content (vol %)	Hydrogen content (mass %)	Carbon content (mass %)	EI(CO_2) (g kg^{-1})	Number of test points*
ECLIF3-1	In-flight	Jet A-1	0.7800	13.4	14.08	85.90	3149	8
	In-flight	HEFA-SPK	0.7618	0.41**	15.11	84.89	3111	11
ECLIF3-2	In-flight & ground-based	Jet A-1	0.7767	13.4	14.25	85.74	3142	25 & 20
	In-flight & ground-based	HEFA-SPK	0.7608	0.02**	15.18	84.82	3108	13 & 13
	Ground-based	Blend	0.7781	10.8	14.39	85.56	3137	12

* For in-flight measurements, test points are defined as plume encounters, and for ground-based measurements, test points are defined as an averaged measurement sequence at stable T3 operating conditions. ** Aromatics content determined by GCxGC analysis in mass %.

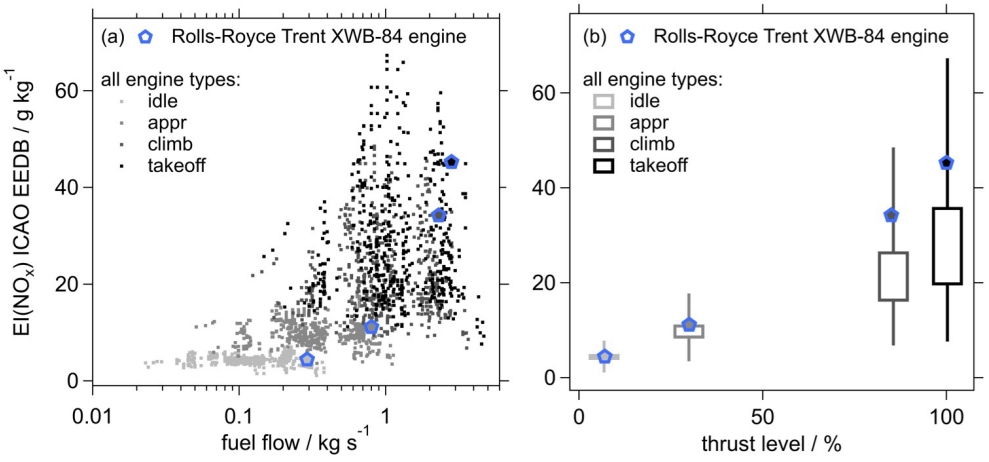

Figure 4. EI(NO_x) based on the entire ICAO Aircraft Engine Emissions Databank v28B (EEDB, 2021). **(a)** shows the dependency of EI(NO_x) on fuel flow, **(b)** on thrust. The values listed for the Rolls-Royce Trent XWB-84 engine, which was the focus during ECLIF3, are highlighted in blue.

approaches exist, which use ground test data and correct them to atmospheric conditions at the respective flight level, flight phase and engine thrust setting, as, for example, done when applying the Rolls-Royce model or fuel flow correlation methods as described in the next section.

2.6 Engine emission prediction methods: P3T3 and fuel flow methods

Based on the set of emissions data determined during the engine certification process, one can derive emission indices over various flight profiles using engine performance and engine emission prediction methods. A modern high-bypass turbofan engine in general follows a Brayton or Joule cycle, where, after a fan, two air streams are separated: in the core of the engine, pressurized air and fuel are burned (temperature is increased by the heat release in the combustion chamber) and are passed through a turbine, and together with the larger bypass air, propulsion thrust is produced. The subsequent positions are characterized and defined by total temperature and pressure regions: T2/P2 at the fan inlet, T24/P24 at the low-pressure compressor outlet, T3/P3 at the high-pressure compressor outlet and T5/P5 at the low-pressure turbine outlet. However, input data such as P3 and T3 are proprietary and thus not publicly available.

Engine performance data or models can be used to directly predict emissions at altitude, which is called the P3T3 method (DuBois and Paynter, 2006). Manufacturers thus have developed their own prediction methods for non-LTO conditions based on correlations derived from empirical rig data to correct for the effect of a change in combustor inlet pressure (P3) and combustor air-to-fuel ratio (AFR) at a fixed combustor inlet temperature (T3). These correlations are typically referred to as P3T3 methods as often the AFR exponent may be set to zero. However, as NO_x sensitivity to AFR depends on the stoichiometric distribution within the combustion zones of a rich burn combustor, it may also be set to some small number to reflect more EI(NO_x) at richer AFRs (towards higher power), as done for this comparison where AFR is set to 0.5. The validation of these methods has proven to be accurate within 10 %.

The EI(NO_x) must further be corrected to the lower pressure at altitude compared to sea-level static $(P3_{\text{sealevel}}/P3_{\text{altitude}})^y$. The exponent y is unique for every engine and derived by the manufacturers but commonly ranges between 0.2 and 0.5 with typically 0.5 for a rich burn combustor being used. In addition, NO_x emissions are also dependent on the ambient humidity as the additional heat capacity of the water reduces combustion temperature and thus the NO_x formation rate. Either actual humidity measurements are needed or a reference humidity of 60 % is assumed (ISO 5878). In-flight measurements of relative humidity in the ECLIF3 test areas show values between 30 % and 70 %; hence the reference value is a reasonable assumption. However, this relative humidity at cold ambient temperature at altitude relates to a much lower absolute humidity by mass compared to ground reference condition of 6.34 g kg^{-1}. Based on the certification humidity correction formula for EI(NO_x), cruise predictions must include a humidity correction of around +12 %.

The direct P3T3 method requires proprietary engine data, which are not available for modellers. Simplified methods were developed to estimate NO_x emissions relating in-flight fuel flow at altitude to publicly available fuel flow data and corresponding EI(NO_x) in the ICAO Aircraft Engine Emissions Databank. Such fuel flow methods (FFMs) provide corrections to the different flight conditions such as altitude, humidity and Mach number (Deidewig et al., 1996; Döpelheuer and Lecht, 1999; DuBois and Paynter, 2006). The ground-based values, as reported by the ICAO Aircraft Engine Emis-

Table 2. Normalization of source engine parameters.

Abbreviation	Parameter	Unit	State within individual test points
ΔT3	total temperature at HPC exit relative change to a representative mission value	K	controlled adjustment
ΔP3	total pressure at HPC exit relative change to a representative mission value	%	changes with T3 adaptations
ΔFF	fuel flow rate per engine relative change to a representative mission value	%	changes with T3 adaptations
Mach	Mach number ratio of true air speed (TAS) and local speed of sound	–	constant
T2	total temperature at fan intake	%	constant

sions Databank, are logarithmically fitted with respect to fuel flow. For EI(NO_x), a power function fit leading to linear relations in a log–log plot is used between two points. Previously published comparisons with in-flight NO_x measurements of older engines have shown that predictions based on fuel flow models and in-flight measurements agreed on average within ±12 % (Schulte et al., 1997). For conventional rich burn combustors, fuel flow methods like Boeing FFM2 (DuBois and Paynter, 2006) are able to predict altitude emissions within 10 % compared to the full proprietary P3T3 method (Norman et al., 2003; SAE, 2009).

In this study, we use the calculated EI(NO_x) of three different engine emission prediction methods and compare them to the 300 in-flight measurements: (a) the Boeing Fuel Flow Method 2 (BFFM2) with which Rolls-Royce estimated EI(NO_x) at the tested operating conditions, (b) an adapted method (aptFFM2) based on the Fuel Flow Method2 (DuBois and Paynter, 2006)[1], and (c) the Rolls-Royce in-house P3T3 method (P3T3). For the fuel flow, actual measurement data and the EI(CO2), according to Table 1, served as input. Differences between the aptFFM2 and BFFM2 method are that the aptFFM2 method uses total pressure and temperature, therefore calculating the effect of aircraft speed, while the BFFM2 method uses ambient pressure and Mach number (Schaefer, 2012).

3 Results and discussion

In-flight measurements aboard the DLR research aircraft *Falcon* were carried out in the framework of the ECLIF3 project in 2021. Based on these in-flight measurements at high altitudes we quantify exhaust emissions by inferring emission indices of NO_x valid for the young exhaust of a long-range Airbus A350-941 aircraft with latest-generation Rolls-Royce Trent XWB-84 engines. For the first time, the Airbus aircraft was fuelled with 100 % HEFA-SPK (Airbus, 2021b, a; Rolls-Royce, 2021). The aircraft was able to switch between Jet A-1 and HEFA-SPK during the flight mission; hence, the impact of fuel effects could be measured in comparable atmospheric conditions. Furthermore, different engine power settings, e.g. compressor exit temperatures and pressure, as well as engine fuel flows or fuel-to-air ratio, were studied at high altitudes. Due to the confidential nature of detailed aircraft and engine parameters, we do not relate the derived emission indices to absolute values of engine sensitive parameters but use a delta notation (Δ) to a representative observed value of the flight mission.

3.1 In-flight ECLIF3 NO_x emission indices

The emitted NO_x of an aircraft engine is dependent on actual thrust and resulting combustor conditions as inlet temperature T3 and pressure P3, as well as local air-to-fuel ratio. Hence, we present EI(NO_x) values depending on different source engine parameters, as listed in Table 2.

Since the temperature at the exit of the high-pressure compressor (HPC), T3, is one of the major parameters affecting emissions, engine throttle was set in order to achieve various levels of T3 in the cruise range (low-, mid- and high-power cruise). This led to different P3 and fuel flow levels, while Mach number and T2 were held roughly constant during different test points by adjusting the second engine.

The dots in Fig. 5a show emission indices derived from near-field measurements on 19 November 2021 at flight level (FL) 310 for varying ΔT3. Two different T3 settings and fuel types (Jet A-1 and 100 % HEFA-SPK) were probed during that flight. The flight altitude (9465 ± 10 m), Mach number (0.62 ± 0.003) and T2 (±1 %) were held constant within the different test points, while T3 was increased by ∼ 40 K. This led to a simultaneous increase in P3 by ∼ 19 % and fuel flow by ∼ 26 %. First, at ΔT3 of approx. −40 K, the mean EI(NO_x) values from Jet A-1 ($16.2 \pm 0.3\,g\,kg^{-1}$) and HEFA-SPK ($15.6 \pm 0.2\,g\,kg^{-1}$) agree within their error estimates. Hence, no statistically significant impact of fuel type on EI(NO_x) can be detected, although the increased hydrogen content of HEFA-SPK could have an impact on the flame temperature and therefore on the NO_x emissions (Gleason and Martone, 1980; Lefebvre, 1984; Yelugoti and Wang, 2023; Alabaş and Çeper, 2024). Second, the mean EI(NO_x) for Jet A-1 increases over the T3 range by ∼ 20 % (to $19.1 \pm 0.4\,g\,kg^{-1}$) and the mean EI(NO_x) for HEFA-SPK by ∼ 17 % (to $18.3 \pm 1.7\,g\,kg^{-1}$). Therefore, it can also be concluded that both fuels show similar sensitivities to combustion conditions as temperature and pressure as expected.

The squares in Fig. 5a represent measurements on 14 and 16 April 2021 at FL360 to underline the two measurements

[1] As coded in December 2022 in Python by Roger Teoh and Marc Stettler at Imperial College, described in Teoh et al. (2022) and converted in 2022 to Fortran by our team at DLR.

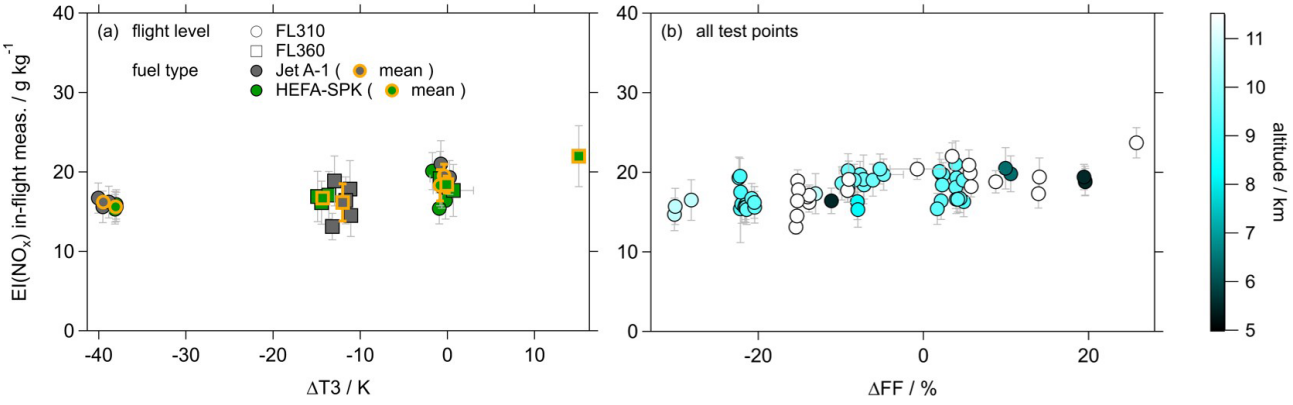

Figure 5. EI(NO_x) as calculated from near-field in-flight measurements behind the Airbus A350-941 with Rolls-Royce Trent XWB-84 engines **(a)** versus desensitized ΔT3 at constant conditions at FL310 and FL360 and **(b)** versus desensitized ΔFF (fuel flow), colour-coded by altitude.

above with additional measurement points on a different day and at different flight altitude. At the ΔT3 setting of approx. −15 K the mean EI(NO_x) values for Jet A-1 and HEFA-SPK again agree within uncertainties. HEFA-SPK, in addition, was probed at two higher T3 settings (approx. 0 K and approx. 15 K) and also shows an increasing trend in mean EI(NO_x) from 16.7 ± 0.5 to 18.4 ± 1 and $22.0\,g\,kg^{-1}$. The spread of individual EI(NO_x) in Fig. 5a may be due to sensitivity of NO_x to ambient conditions. The standard deviations from the means in EI(NO_x) for FL310 are between 3 %–8 % for Jet A-1 and around 2 %–11 % for HEFA-SPK. The standard deviations from the means for EI(NO_x) for FL360 are up to 15 % for Jet A-1 and 3 %–6 % for HEFA-SPK. However, these internal variabilities are still smaller than the increasing trend of the mean values with T3.

Figure 5b presents data points acquired during the ECLIF3 experiment plotted against fuel flow range and colour-coded by flight altitude. Despite the scattered data, the expected increase in NO_x emissions with increasing fuel flow can be recognized. Due to the multi-dimensional dependency of EI(NO_x) on more than one engine parameter we cannot further assess the relative importance of individual engine parameter changes. However, we do not observe differences for the different flight altitudes where the measurements took place.

3.2 Comparison of in-flight ECLIF3 NO_x emission indices with engine emission prediction methods

In this section, we compare our near-field ECLIF3 in-flight measurements with predictions. Please note that all ECLIF3-1 and ECLIF3-2 test points were analysed using BFFM2 and aptFFM2, whereas P3T3 method results are only available for ECLIF3-2. The uncertainty for BFFM2 is around 10 % (DuBois and Paynter, 2006); for aptFFM2 ∼20% (ICAO, 2020; Teoh et al., 2022); for P3T3 around 10 % to 15 % (SAE, 2009); and for the in-flight-measured EI(NO_x) ∼14%, as derived from emission index uncertainty analysis below (see Sect. 3.4).

In general, the measurement to engine emission prediction method agreement is good with a correlation coefficient (R^2) of 0.3 to 0.4. For aptFFM2, BFFM2 and P3T3, roughly 40 %, 50 % and 75 % of data points agree within a difference of $\pm 3\,g\,kg^{-1}$ and are thus well within the combined errors of prediction method results and in-flight measurements. Deviations between the methods are within the error limits. However, predicted EI(NO_x) values tend to be on average ∼15 % (aptFFM2, P3T3) to ∼20 % (BFFM2) lower than calculated EIs from the in-flight measurements in near field conditions. Figure 6 shows, analogous to Fig. 5a, that only data points for constant flight conditions at FL310 and FL360 with a focus on the ΔT3 setting of 0 K. This subset focuses on a set of conditions for which the DISA was quite similar; hence the atmospheric temperature conditions do not affect the emission indices. Still, the predictions tend to show smaller EI(NO_x) than determined by the in-flight measurements of the engines at cruise at slightly lower Mach numbers compared to typical cruise conditions.

3.3 Ground-based ECLIF3-2 NO_x emission indices

The ground-based measurements behind the Rolls-Royce Trent XWB-84 engine were performed on 2 d at similar ambient temperatures. The reference measurements with fossil Jet A-1 were performed on 22 October 2021 (temperature: 12.2–14.4 °C; relative humidity: 87 %–81 % during test run). The neat HEFA-SPK and an additional fuel blend (HEFA-SPK blended with a different Jet A-1) were tested on 23 October 2021 (temperature: 9.1–15.2 °C; relative humidity: 47 %–96 % during test run). The hydrogen content and carbon content by mass % of the blend are 14.39 % and 85.61 %, respectively (see Table 1). Four test points with Jet A-1 were repeated on the second day in order to identify any biases from changes in environmental conditions or different

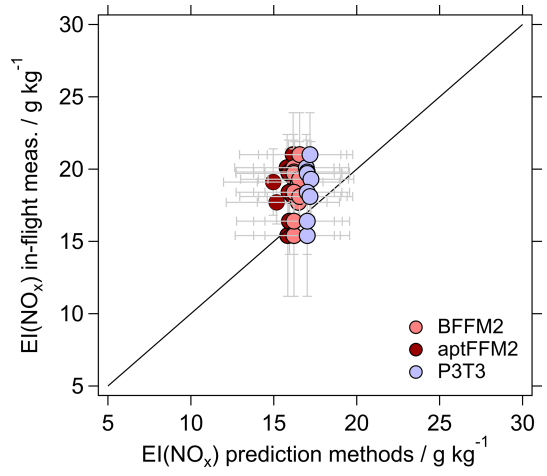

Figure 6. EI(NO_x) from ECLIF3 in-flight measurements and three prediction estimates for the 0 K ΔT3 setting at FL310 and FL360. Engine emission prediction methods use the EI(NO_x) from the ground-based ICAO Aircraft Engine Emissions Databank. The black line marks the 1 : 1 agreement.

probe alignment. The engine was operated at several different power settings, ranging from idle conditions to maximum climb.

Thus, the ground-based measurements allow the detection of the EI(NO_x) curve over a larger range of T3 and fuel flow (see Fig. 7). The EI(NO_x) emission curve shows a continuous increase with higher thrust and corresponding increasing T3, P3 and fuel flow. As expected and discussed above, NO_x emissions are not significantly affected by the fuel composition. The measured EI(NO_x) values for the different fuel types agree within estimated error margins. These findings are in line with results of ground-based measurements behind an Airbus A320-232 with IAE V2527-A5 engines in 2018 using fossil Jet A-1 fuels as well as blends of HEFA-SPK and Jet A-1 as discussed by Schripp et al. (2022). They also found an independence of NO_x emissions on fuel type and similar sensitivities to combustion temperature ($\Delta T3 \sim 40$ K, $\Delta EI(NO_x) \sim 4\,g\,kg^{-1}$). Bulzan et al. (2010) also presented and discussed NO_x emissions of a ground-based experiment in 2009 targeting the CFM56-2C1 engine of the NASA DC-8 aircraft burning pure fossil fuels (JP-8) as well as blends with Fischer–Tropsch fuels based on natural gas and coal. They found an increase in EI(NO_x) with fuel flow by about $\sim 6\,g\,kg^{-1}$ per $\sim 100\,\%$ more burned fuel, which is in line with the measurements performed in this study.

Figure 8 compares EI(NO_x) from far-field in-flight measurements with P3T3 and BFFM2 engine emission prediction methods that use the ECLIF3-2 ground-based measurements of the same Rolls-Royce Trent XWB-84 engine as input (see Fig. 7). Using the engine emission prediction methods, the ECLIF3-2 ground-based measurements are related to in-flight conditions and cruise altitudes, i.e. to lower pressure and absolute humidity compared to the ground. Although lower absolute humidity should increase NO_x by 12 %, in general, the prediction methods are expected to show lower NO_x levels compared to the ground-based measurements due to the lower pressure at altitude. The predictions are compared to ECLIF3-2 far-field measurements, where the Airbus A350-941 and the *Falcon* were flying at typical cruise conditions and Mach numbers. The two engine emission prediction methods agree well with the measurements at cruise altitudes within the estimated uncertainties. The BFFM2 predictions are typically 10 % higher compared to P3T3 methods, which has been found before for this type of combustor but is still within the ΔT3 ranges. The agreement between the prediction methods and the in-flight measurements is significantly improved using the ground-based EI(NO_x) measurements on the same engine instead of using data from the ICAO Aircraft Engine Emissions Databank, as was done for the comparison in Fig. 6. The use of ECLIF3-2 ground-based measurement data on the same engine considers a potential slight change in engine performance of well-maintained in-operation engines. The comparison to in-flight measurements at typical cruise conditions in terms of T3, P3, AFR and Mach number also ensures a better comparability of the predictions well within the range tested in rig tests.

3.4 In-flight emission index uncertainty analysis

Here, we present an in-depth analysis of different aspects contributing to the uncertainty of each individual inferred emission index (see Eq. 1) with respect to the in-flight measurements. The EI(NO_x) uncertainty consists of several individual errors: (a) the uncertainty of the enhancement above an atmospheric background level ($\partial(\Delta NO_y)$ and $\partial(\Delta CO_2)$), which can be subdivided into (a.a) the absolute accuracy of the measured species (∂NO_{y_acc}, ∂CO_{2_acc}) and (a.b) the uncertainty related to the atmospheric background determination (∂NO_{y_bgr}, ∂CO_{2_bgr}); (b) the uncertainty in EI(CO_2); and (c) the uncertainty in the molar masses of NO_2 and CO_2. The total uncertainty ($\partial EI(NO_x)$) is then estimated using Gaussian error propagation following Eq. (3):

$$\begin{aligned}\partial EI(NO_x) = \pm \Bigg[& \left(\frac{\partial EI(NOx)}{\partial NO_y}\partial NO_{y\_acc}\right)^2 + \left(\frac{\partial EI(NO_x)}{\partial NO_y}\partial NO_{y\_bgr}\right)^2 \\ & + \left(\frac{\partial EI(NO_x)}{\partial CO_2}\partial CO_{2\_acc}\right)^2 + \left(\frac{\partial EI(NO_x)}{\partial CO_2}\partial CO_{2\_bgr}\right)^2 + \\ & + \left(\frac{\partial EI(NO_x)}{\partial EI(CO_2)}\partial EI(CO_2)\right)^2 + \left(\frac{\partial EI(NO_x)}{\partial M(NO_2)}\partial M(NO_2)\right)^2 \\ & + \left(\frac{\partial EI(NO_x)}{\partial M(CO_2)}\partial M(CO_2)\right)^2 \Bigg]^{\frac{1}{2}}. \end{aligned} \quad (3)$$

The individual uncertainty terms and the total uncertainty for EI(NO_x) are listed in Table 3. For EI(NO_x) the mean uncertainty from all in-flight plume encounters sums up to ∼ 14 %. Figure 9 further depicts the relative contribution of the individual terms to the total uncertainty for each plume encounter. It is evident that the most important uncertainty term

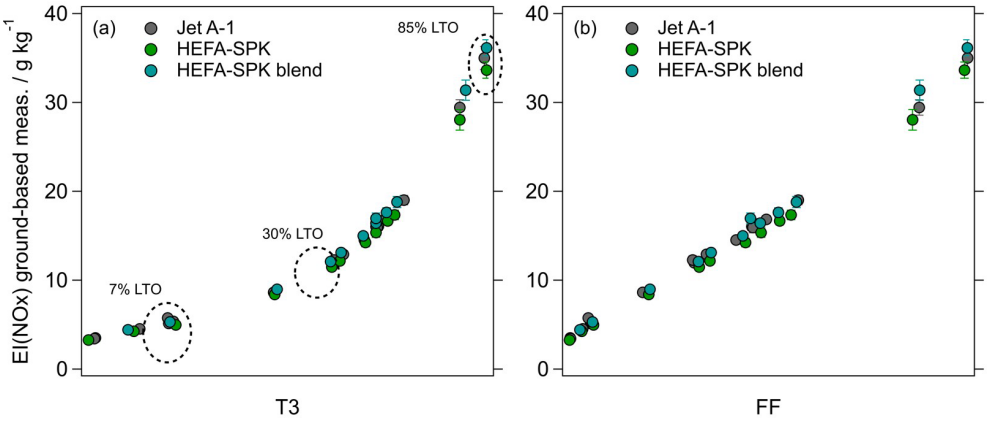

Figure 7. EI(NO_x) from ECLIF3-2 ground-based measurements behind the Airbus A350-941 with Rolls-Royce Trent XWB-84 engines versus T3 (referenced to 60 % RH, **(a)**) and FF (fuel flow) **(b)** for Jet A-1, HEFA-SPK and blend. Values on the x axis are undisclosed. Black circles indicate LTO points.

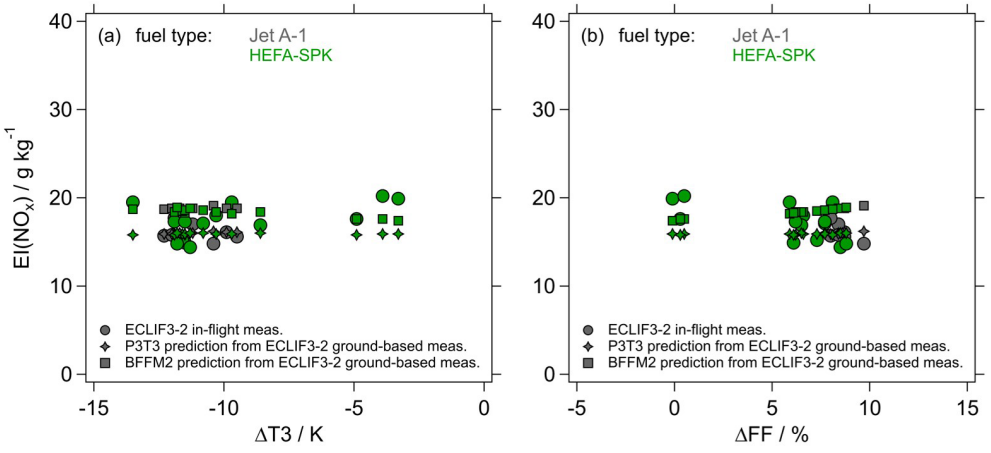

Figure 8. EI(NO_x) (dots) from ECLIF3-2 in-flight measurements for different fuels at typical cruise Mach numbers in the far-field at FL320 and FL350 from behind the Airbus A350-941 with Rolls-Royce Trent XWB-84 engines versus desensitized ΔT3 **(a)** and desensitized ΔFF (fuel flow) **(b)**. Predicted EI(NO_x) for the far-field measurement conditions from the P3T3 prediction method and the BFFM2 prediction method calculated based on ECLIF3-2 ground-based measurements shown in Fig. 7.

for EI(NO_x) is the NO_y accuracy. For future aircraft experiments we plan to implement a different dilution approach and suggest flying in a larger distance to the aircraft of interest to prevent the instrument from running into saturation effects.

The measurement uncertainties, i.e. the measurement accuracies for NO_y and CO_2, were described in Sect. 2.1, including errors from the individual instruments, measurement techniques and calibration procedures. These absolute measurement accuracies (in ppb and ppm) are then translated into a relative accuracy (in %) based on the maximum mixing ratio enhancement observed during each exhaust plume encounter. The mean relative accuracy for CO_2 is < 1 % (0.1 %–2.5 %) and for NO_y 13 % (9 %–23 %); see Table 3. The contribution of the individual accuracy of NO_y or CO_2 is generally higher (lower) when the encountered mixing ratio enhancement was low (high). The uncertainty of EI(CO_2), as

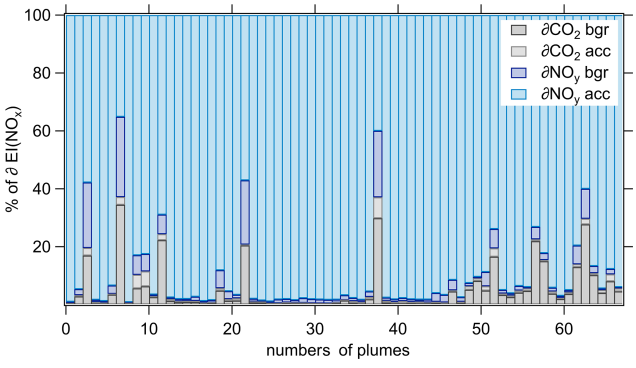

Figure 9. Stacked relative individual uncertainties contributing to the total uncertainty ∂EI(NO_x) for in-flight plume encounters.

Table 3. Individual contributions to the total uncertainty $\partial \mathrm{EI}(\mathrm{NO}_x)$ for all in-flight exhaust encounters. The table denotes mean values; however, the uncertainty is estimated for each individual plume encounter individually.

Uncertainty term	Mean uncertainty estimate (%)
$\partial \mathrm{NO}_y$acc	13
$\partial \mathrm{NO}_y$bgr	< 1
$\partial \mathrm{CO}_2$acc	< 1
$\partial \mathrm{CO}_2$bgr	1
$\partial \mathrm{EI}(\mathrm{CO}_2)$	0.1
$\partial M(\mathrm{NO}_2)$	0.002
$\partial M(\mathrm{CO}_2)$	0.003
∂ EI(NO_x)	14
Total uncertainty	

well as of the molar masses, is negligible. The atmospheric background mole fraction needs to be determined for each individual plume encounter individually to account for horizontal, vertical and temporal gradients in the ambient atmosphere. However, the typical atmospheric background variation of NO_y (4 ppb) and CO_2 (5 ppm) is not sensitive to the high mixing ratios encountered ($\Delta\mathrm{NO}_y \sim 500$–$4000$ ppb, $\Delta\mathrm{CO}_2 \sim 100$–$800$ ppm). The atmospheric background itself is estimated based on the following assumption. Primarily, prior to and after the plume encounter, the probed air mass needs to be free of engine exhaust. Due to the natural dynamics of the troposphere, the atmospheric background for the long-lived gases CO_2 is not always as obvious as in the short-lived NO_y; hence, NO_y is taken as the main focus for this determination. If prior to and after the encounter the mole fractions are identical, this value is taken for the atmospheric background. If the mole fractions are different, the atmospheric background is set in between these values. The mean difference from the mixing ratio at the start and end of the individual plume encounter to the respective atmospheric background estimate is considered in the uncertainty of the atmospheric background estimate. Moreover, the standard deviation (1σ) of an atmospheric background-like sequence is considered.

4 Conclusions

In conclusion, we presented the first $\mathrm{EI}(\mathrm{NO}_x)$ in-flight measurements for a modern long-range aircraft and engines since 1995 (Schulte et al., 1997). We showed that the measurements and methodology are adequate to infer $\mathrm{EI}(\mathrm{NO}_x)$ emissions from aircraft at high altitudes. As expected from previous ground engine tests, the fuel type, even a 100 % HEFA-SPK, has no statistically significant effect on the NO_x emission index. $\mathrm{EI}(\mathrm{NO}_x)$ increases with increasing combustion temperature, pressure and fuel flow for the measured cruise T3 range conditions. Furthermore, the in-flight measurements generally agree with predictions from three different engine emission prediction methods within combined uncertainties when using data sets from the ground-based ICAO Aircraft Engine Emissions Databank as input, with a slight trend towards modelled lower emission indices. In order to consider performance variations of the operational engines during maintenance cycles and to avoid engine to engine performance variations, we performed ground measurements behind the same engine over a wide T3 range. The ground-based measurements show an increase in $\mathrm{EI}(\mathrm{NO}_x)$ with increasing thrust, as explained by higher combustor temperatures. The ground-based measurements were then used as input to predict $\mathrm{EI}(\mathrm{NO}_x)$ at cruise altitudes for typical cruise conditions using current engine emission prediction methods. The methods generally agree better with the measured $\mathrm{EI}(\mathrm{NO}_x)$ for in-flight measurements at typical cruise conditions with respect to P3, T3, AFR and Mach number. These experiments present the first in-flight measurements targeting NO_x emissions of latest-generation engines at high altitudes and thus provide a valuable data set of $\mathrm{EI}(\mathrm{NO}_x)$ cruise measurements for the evaluation of state-of-the art engine emission prediction methods. The measurements thereby enhance the sparse existing data set of cruise emissions of older-generation engines.

Data availability. The CO_2 and NO_y flight measurement data are released at https://doi.org/10.5281/zenodo.10646359 (Harlass et al., 2024).

Author contributions. TH analysed the NO_y and CO_2 measurement data and wrote the manuscript with inputs from all co-authors. TH, RD, RM, DS, MS, SK and PSt performed the *Falcon* measurements. TS, TG and LB performed the ground-based measurements. CV and CR conceived and designed the aircraft experiments. US, MJ, DL, DA and PM performed the model simulations. All authors contributed to the interpretation of the data, reviewed the manuscript and gave their approval of the final paper.

Competing interests. Charles Renard and Maxime Gauthier are employed by Airbus Operations SAS. Mark Johnson, Darren Luff, Paul Madden and Peter Swann are employed by Rolls-Royce plc. and Denise Ahrens by Rolls-Royce Deutschland. Reetu Sallinen is employed by Neste Corporation. All other authors declare that they have no conflict of interest.

Acknowledgements. The authors especially thank DLR-FX for the experiment cooperation. This involves not only our pilots Michael Grossrubatscher, Thomas von Marwick, Philipp Weber and Roland Welser but also the management Georg Dietz and Oliver Paxa and the group of Martin Zöger, Andreas Giez, Vladyslav Nenakhov, Christoph Grad, Marina Schimpf, Christian Mallaun, David Woudsma, Alexander Wolf, Frank Probst, Stefan Hempe and many more. We also thank the flight test team of Airbus for the great coordination of the aircraft on ground as well as in the test areas. Great recognition is dedicated to the Rolls-Royce Technical Support team in Toulouse. And a special word of thanks is dedicated to all other ECLIF3 partners for their helpful cooperation. The first author really appreciates the great effort of Tiziana Bräuer and Magdalena Pühl, who finished the manuscript and answered the reviewer comments during the parental leave of Theresa Harlass.

Financial support. This research has been supported by the Deutsche Forschungsgemeinschaft, DFG (grant nos. 510826369 and 522359172), and by the European Union (grant agreement nos. 101101999 and 101114613).

The article processing charges for this open-access publication were covered by the German Aerospace Center (DLR).

Review statement. This paper was edited by Fangqun Yu and reviewed by three anonymous referees.

References

Airbus: An A350 fuelled by 100 % SAF just took off, 18 March 2021, https://www.airbus.com/en/newsroom/stories/2021-03-an-a350-fuelled-by-100-saf-just-took-off (last access: 25 August 2023), 2021a.

Airbus: First in-flight 100 % sustainable-fuels emissions study of passenger jet shows early promise, Toulouse, 29 November 2021, https://www.airbus.com/en/newsroom/press-releases/2021-11-first-in-flight-100 (last access: 15 May 2023), 2021b.

Alabaş, H. A. and Çeper, B., A.: Effect of the hydrogen/kerosene blend on the combustion characteristics and pollutant emissions in a mini jet engine under CDC conditions, Int. J. Hydro. Energy, 52 B, 1275–1287, ISSN 0360-3199, https://doi.org/10.1016/j.ijhydene.2023.05.146, 2024.

Bollinger, M. J., Sievers, R. E., Fahey, D. W., and Fehsenfeld, F. C.: Conversion of nitrogen dioxide, nitric acid, and n-propyl nitrate to nitric oxide by a gold-catalyzed reduction with carbon monoxide, Anal. Chem., 55, 1980–1986, https://doi.org/10.1021/ac00262a034, 1983.

Bradshaw, J., Davis, D., Grodzinsky, G., Smyth, S., Newell, R., Sandholm, S., and Liu, S.: Observed distributions of nitrogen oxides in the remote free troposphere from the Nasa Global Tropospheric Experiment Programs, Rev. Geophys., 38, 61–116, https://doi.org/10.1029/1999RG900015, 2000.

Brasseur, G. P., Müller, J.-F., and Granier, C.: Atmospheric impact of NO_x emissions by subsonic aircraft: A three-dimensional model study, J. Geophys. Res.-Atmos., 101, 1423–1428, https://doi.org/10.1029/95JD02363, 1996.

Bräuer, T., Voigt, C., Sauer, D., Kaufmann, S., Hahn, V., Scheibe, M., Schlager, H., Huber, F., Le Clercq, P., Moore, R. H., and Anderson, B. E.: Reduced ice number concentrations in contrails from low-aromatic biofuel blends, Atmos. Chem. Phys., 21, 16817–16826, https://doi.org/10.5194/acp-21-16817-2021, 2021a.

Bräuer, T., Voigt, C., Sauer, D., Kaufmann, S., Hahn, V., Scheibe, M., Schlager, H., Diskin, G. S., Nowak, J. B., DiGangi, J. P., Huber, F., Moore, R. H., and Anderson, B. E.: Airborne Measurements of Contrail Ice Properties – Dependence on Temperature and Humidity, Geophys. Res. Lett., 48, e2020GL092166, https://doi.org/10.1029/2020GL092166, 2021b.

Bulzan, D., Anderson, B., Wey, C., Howard, R., Winstead, E., Beyersdorf, A., Corporan, E., DeWitt, M. J., Klingshirn, C., Herndon, S., Miake-Lye, R., Timko, M., Wood, E., Tacina, K. M., Liscinsky, D., Hagen, D., Lobo, P., and Whitefield, P.: Gaseous and Particulate Emissions Results of the NASA Alternative Aviation Fuel Experiment (AAFEX), ASME Turbo Expo 2010: Power for Land, Sea, and Air, 1195–1207, https://doi.org/10.1115/gt2010-23524,

Dahlmann, K., Grewe, V., Ponater, M., and Matthes, S.: Quantifying the contributions of individual NO_x sources to the trend in ozone radiative forcing, Atmos. Environ., 45, 2860–2868, https://doi.org/10.1016/j.atmosenv.2011.02.071, 2011.

Deidewig, F., Döpelheuer, A., and Lecht, M.: Methods to assess aircraft engine emissions in flight, ICAS PROCEEDINGS, 131–141, 1996.

Döpelheuer, A. and Lecht, M.: Influence of engine performance on emission characteristics, paper no. 20 in "Gas Turbine Engine Combustion, Emissions and Alternative Fuels", RTO-MP-14, ISBN 92-837-0009-0, Lisbon, 1999.

Drummond, J. W., Volz, A., and Ehhalt, D. H.: An optimized chemiluminescence detector for tropospheric NO measurements, J. Atmos. Chem., 2, 287–306, https://doi.org/10.1007/BF00051078, 1985.

DuBois, D. and Paynter, G. C.: "Fuel Flow Method2" for Estimating Aircraft Emissions, SAE Technical Paper 2006-01-1987, https://doi.org/10.4271/2006-01-1987, 2006.

EEDB: ICAO Aircraft Engine Emissions Databank v28B, https://www.easa.europa.eu/en/domains/environment/icao-aircraft-engine-emissions-databank (last access: January 2023), 2021.

Fahey, D. W., Eubank, C. S., Hübler, G., and Fehsenfeld, F. C.: Evaluation of a catalytic reduction technique for the measurement of total reactive odd-nitrogen NOyin the atmosphere, J. Atmos. Chem., 3, 435–468, https://doi.org/10.1007/BF00053871, 1985.

Fiehn, A., Kostinek, J., Eckl, M., Klausner, T., Gałkowski, M., Chen, J., Gerbig, C., Röckmann, T., Maazallahi, H., Schmidt, M., Korbeń, P., Nęcki, J., Jagoda, P., Wildmann, N., Mallaun, C., Bun, R., Nickl, A.-L., Jöckel, P., Fix, A., and Roiger, A.: Estimating CH_4, CO_2 and CO emissions from coal mining and industrial activities in the Upper Silesian Coal Basin using an aircraft-based mass balance approach, Atmos. Chem. Phys., 20, 12675–12695, https://doi.org/10.5194/acp-20-12675-2020, 2020.

Gleason, C. C. and Martone, J. A.: Fuel character effects on j79 and f101 engine combustor emissions, J. Energy, 4, 223–226, https://doi.org/10.2514/3.62477, 1980.

Gokulakrishnan, P. and Klassen, M. S.: NOx and CO Formation and Control, in: Gas Turbine Emissions, edited

by: Lieuwen, T. C. and Yang, V., Cambridge Aerospace Series, Cambridge University Press, Cambridge, 175–208, https://doi.org/10.1017/CBO9781139015462.011, 2013.

Grewe, V., Matthes, S., and Dahlmann, K.: The contribution of aviation NOx emissions to climate change: are we ignoring methodological flaws?, Environ. Res. Lett., 14, 121003, https://doi.org/10.1088/1748-9326/ab5dd7, 2019.

Harlass, T., Scheibe, M., and Roiger, A.: CO_2 and NO_y aircraft measurement data obtained within the framework of the ECLIF3 campaign, Zenodo [data set], https://doi.org/10.5281/zenodo.10646359, 2024.

ICAO: Annex 16 to the Convention on International Civil Aviation, Environmental Protection, Volume II Aircraft Engine Emissions, Fourth Edition, July 2017, ISBN 978-92-9258-314-9, 2017.

ICAO: Airport Air Quality Manual, Doc 9889, Second Edition, ISBN 978-92-9258-963-9, 2020.

ICAO: ICAO Aircraft Engine Emissions Databank v29, February 2023, https://www.easa.europa.eu/en/domains/environment/icao-aircraft-engine-emissions-databank (last access: 4 May 2023), 2023.

IPCC: Prepared in collaboration with the Scientific Assessment Panel to the Montreal Protocol on Substances that Deplete the Ozone Layer Cambridge University Press, edited by: Penner, J. E., Lister, D. H., Griggs, D. J., Dokken, D. J., and McFarland, M., UK, 373 pp., available from Cambridge University Press, The Edinburgh Building Shaftesbury Road, Cambridge CB2 2RU ENGLAND, 1999.

IPCC: Climate Change 2021: The Physical Science Basis. Contribution of Working Group I to the Sixth Assessment Report of the Intergovernmental Panel on Climate Change, Cambridge University Press, Cambridge, United Kingdom and New York, NY, USA, https://doi.org/10.1017/9781009157896, 2021.

Jurkat, T., Voigt, C., Arnold, F., Schlager, H., Kleffmann, J., Aufmhoff, H., Schäuble, D., Schaefer, M., and Schumann, U.: Measurements of HONO, NO, NO_y and SO_2 in aircraft exhaust plumes at cruise, Geophys. Res. Lett., 38, L10807, https://doi.org/10.1029/2011GL046884, 2011

Kärcher, B., Hirschberg, M. M., and Fabian, P.: Small-scale chemical evolution of aircraft exhaust species at cruising altitudes, J. Geophys. Res.-Atmos., 101, 15169–15190, https://doi.org/10.1029/96JD01059, 1996.

Klausner, T., Mertens, M., Huntrieser, H., Galkowski, M., Kuhlmann, G., Baumann, R., Fiehn, A., Jöckel, P., Pühl, M., and Roiger, A.: Urban greenhouse gas emissions from the Berlin area: A case study using airborne CO_2 and CH_4 in situ observations in summer 2018, Elementa: Sci. Anthropo., 8, 15, https://doi.org/10.1525/elementa.411, 2020.

Klausner, T. M.: Aircraft-based in situ measurements of CH_4 and CO_2 downstream of European and Asian urban centres at local to synoptic scales, lmu, https://doi.org/10.5282/edoc.26983, 2020.

Kleine, J., Voigt, C., Sauer, D., Schlager, H., Scheibe, M., Jurkat-Witschas, T., Kaufmann, S., Kärcher, B., and Anderson, B. E.: In Situ Observations of Ice Particle Losses in a Young Persistent Contrail, Geophys. Res. Lett., 45, 13553–513561, https://doi.org/10.1029/2018GL079390, 2018.

Köhler, M. O., Rädel, G., Dessens, O., Shine, K. P., Rogers, H. L., Wild, O., and Pyle, J. A.: Impact of perturbations to nitrogen oxide emissions from global aviation, J. Geophys. Res.-Atmos., 113, D11305, https://doi.org/10.1029/2007JD009140, 2008.

Lavoie, G. A., Heywood, J. B., and Keck, J. C.: Experimental and Theoretical Study of Nitric Oxide Formation in Internal Combustion Engines, Combust. Sci. Technol., 1, 313–326, https://doi.org/10.1080/00102206908952211, 1970.

Le Quéré, C., Jackson, R. B., Jones, M. W., Smith, A. J. P., Abernethy, S., Andrew, R. M., De-Gol, A. J., Willis, D. R., Shan, Y., Canadell, J. G., Friedlingstein, P., Creutzig, F., and Peters, G. P.: Temporary reduction in daily global CO_2 emissions during the COVID-19 forced confinement, Nat. Clim. Change, 10, 647–653, https://doi.org/10.1038/s41558-020-0797-x, 2020.

Lee, B. H., Santoni, G. W., Wood, E. C., Herndon, S. C., Miake-Lye, R. C., Zahniser, M. S., Wofsy, S. C., and Munger, J. W. : Measurements of Nitrous Acid in Commercial Aircraft Exhaust at the Alternative Aviation Fuel Experiment, Environ. Sci. Technol. 45, 7648–7654, https://pubmed.ncbi.nlm.nih.gov/21809872/ (last access: January 2023), 2011.

Lee, D. S., Pitari, G., Grewe, V., Gierens, K., Penner, J. E., Petzold, A., Prather, M. J., Schumann, U., Bais, A., Berntsen, T., Iachetti, D., Lim, L. L., and Sausen, R.: Transport impacts on atmosphere and climate: Aviation, Atmos. Environ., 44, 4678–4734, https://doi.org/10.1016/j.atmosenv.2009.06.005, 2010.

Lee, D. S., Fahey, D. W., Skowron, A., Allen, M. R., Burkhardt, U., Chen, Q., Doherty, S. J., Freeman, S., Forster, P. M., Fuglestvedt, J., Gettelman, A., De León, R. R., Lim, L. L., Lund, M. T., Millar, R. J., Owen, B., Penner, J. E., Pitari, G., Prather, M. J., Sausen, R., and Wilcox, L. J.: The contribution of global aviation to anthropogenic climate forcing for 2000 to 2018, Atmos. Environ., 244, 117834, https://doi.org/10.1016/j.atmosenv.2020.117834, 2021.

Lefebvre, A. H.: Fuel Effects on Gas Turbine Combustion-Liner Temperature, Pattern Factor, and Pollutant Emissions, J. Aircraft, 21, 887–898, https://doi.org/10.2514/3.45059, 1984.

LI-COR: The Importance of Water VaporMeasurements and Corrections, Tech Tip, https://www.licor.com/env/support/TechTips/irg4110-h2o-measurement.html (last access: January 2023), 2003.

LI-COR: Li-7000 CO_2/H_2O Analyzer, Instruction Manual, Publication Number 984-07364, 222 pages, https://www.licor.com/env/pdf/gas_analyzers/7000/LI-7000Manual.pdf (last access: January 2023), 2007.

Märkl, R. S., Voigt, C., Sauer, D., Dischl, R. K., Kaufmann, S., Harlaß, T., Hahn, V., Roiger, A., Weiß-Rehm, C., Burkhardt, U., Schumann, U., Marsing, A., Scheibe, M., Dörnbrack, A., Renard, C., Gauthier, M., Swann, P., Madden, P., Luff, D., Sallinen, R., Schripp, T., and Le Clercq, P.: Powering aircraft with 100 % sustainable aviation fuel reduces ice crystals in contrails, EGUsphere [preprint], https://doi.org/10.5194/egusphere-2023-2638, 2023.

Moore, R. H., Thornhill, K. L., Weinzierl, B., Sauer, D., D'Ascoli, E., Kim, J., Lichtenstern, M., Scheibe, M., Beaton, B., Beyersdorf, A. J., Barrick, J., Bulzan, D., Corr, C. A., Crosbie, E., Jurkat, T., Martin, R., Riddick, D., Shook, M., Slover, G., Voigt, C., White, R., Winstead, E., Yasky, R., Ziemba, L. D., Brown, A., Schlager, H., and Anderson, B. E.: Biofuel blending reduces particle emissions from aircraft engines at cruise conditions, Nature, 543, 411–415, https://doi.org/10.1038/nature21420, 2017.

Norman, P., Lister, D., Lecht, M., Madden, P., Park, K., Penanhoat, O., Plaisance, C., and Renger, K.: Development of the Technical Basis for a New Emissions Parameter Covering the Whole

AIRcraft Operation: NEPAIR-Final Technical Report; European Commission Project, Report No. GRD1-1999-10439., 2003.

Ridley, B. A. and Howlett, L. C.: An instrument for nitric oxide measurements in the stratosphere, Rev. Sci. Instrum., 45, 742–746, https://doi.org/10.1063/1.1686726, 1974.

Roiger, A., Thomas, J. L., Schlager, H., Law, K. S., Kim, J., Schäfler, A., Weinzierl, B., Dahlkötter, F., Krisch, I., Marelle, L., Minikin, A., Raut, J. C., Reiter, A., Rose, M., Scheibe, M., Stock, P., Baumann, R., Bouarar, I., Clerbaux, C., George, M., Onishi, T., and Flemming, J.: Quantifying Emerging Local Anthropogenic Emissions in the Arctic Region: The ACCESS Aircraft Campaign Experiment, B. Am. Meteorol. Soc., 96, 441–460, https://doi.org/10.1175/BAMS-D-13-00169.1, 2015.

Rolls-Royce: Aviation leaders launch first in-flight 100 % sustainable-fuel emissions study on commercial passenger jet, 18 March 2021, https://www.rolls-royce.com/media/press-releases/2021/18-03-2021-aviation-leaders-launch-first-in-flight-100 (last access: 25 August 2023), 2021.

SAE: SAE Aerospace Information Report, 2009, "AIR5715 Procedure for the Calculation of Aircraft Emissions," SAE International, Warrendale, PA, Report, https://www.sae.org/standards/content/air5715/ (last access: January 2023), 2009.

Schaefer, M. and Bartosch, S.: Overview on fuel flow correlation methods for the calculation of NO_x, CO and HC emissions and their implementation into aircraft performance software, 235 pp., https://elib.dlr.de/77004/ (last access: January 2023), 2013.

Schlager, H., Konopka, P., Schulte, P., Schumann, U., Ziereis, H., Arnold, F., Klemm, M., Hagen, D. E., Whitefield, P. D., and Ovarlez, J.: In situ observations of air traffic emission signatures in the North Atlantic flight corridor, J. Geophys. Res.-Atmos., 102, 10739–10750, https://doi.org/10.1029/96JD03748, 1997.

Schmitt, J.: Aufbau und Erprobung eines in-situ NO/NOy-Mess-Systems am Höhenforschungsflugzeug M55-Geophysica, Dissertation, LMU München, 160 pp., https://elib.dlr.de/49852/ (last access: January 2023), 2003.

Schripp, T., Anderson, B. E., Bauder, U., Rauch, B., Corbin, J. C., Smallwood, G. J., Lobo, P., Crosbie, E. C., Shook, M. A., Miake-Lye, R. C., Yu, Z., Freedman, A., Whitefield, P. D., Robinson, C. E., Achterberg, S. L., Köhler, M., Oßwald, P., Grein, T., Sauer, D., Voigt, C., Schlager, H., and LeClercq, P.: Aircraft engine particulate matter emissions from sustainable aviation fuels: Results from ground-based measurements during the NASA/DLR campaign ECLIF2/ND-MAX, Fuel, 325, 124764, https://doi.org/10.1016/j.fuel.2022.124764, 2022.

Schulte, P. and Schlager, H.: In-flight measurements of cruise altitude nitric oxide emission indices of commercial jet aircraft, Geophys. Res. Lett., 23, 165–168, https://doi.org/10.1029/95GL03691, 1996.

Schulte, P., Schlager, H., Ziereis, H., Schumann, U., Baughcum, S. L., and Deidewig, F.: NO_x emission indices of subsonic long-range jet aircraft at cruise altitude: In situ measurements and predictions, J. Geophys. Res.-Atmos., 102, 21431–21442, https://doi.org/10.1029/97JD01526, 1997.

Schumann, U., Poll, I., Teoh, R., Koelle, R., Spinielli, E., Molloy, J., Koudis, G. S., Baumann, R., Bugliaro, L., Stettler, M., and Voigt, C.: Air traffic and contrail changes over Europe during COVID-19: a model study, Atmos. Chem. Phys., 21, 7429–7450, https://doi.org/10.5194/acp-21-7429-2021, 2021.

Skowron, A., Lee, D. S., De León, R. R., Lim, L. L., and Owen, B.: Greater fuel efficiency is potentially preferable to reducing NO_x emissions for aviation's climate impacts, Nat. Commun., 12, 564, https://doi.org/10.1038/s41467-020-20771-3, 2021.

Stratmann, G.: Stickoxidmessungen in der Tropopausenregion an Bord eines Linienflugzeugs: Großräumige Verteilung und Einfluss des Luftverkehrs, 207 pp., https://elib.dlr.de/89732/ (last access: January 2023), 2013.

Stratmann, G., Ziereis, H., Stock, P., Brenninkmeijer, C. A. M., Zahn, A., Rauthe-Schöch, A., Velthoven, P. V., Schlager, H., and Volz-Thomas, A.: NO and NO_y in the upper troposphere: Nine years of CARIBIC measurements onboard a passenger aircraft, Atmos. Environ., 133, 93–111, https://doi.org/10.1016/j.atmosenv.2016.02.035, 2016.

Teoh, R., Schumann, U., Gryspeerdt, E., Shapiro, M., Molloy, J., Koudis, G., Voigt, C., and Stettler, M. E. J.: Aviation contrail climate effects in the North Atlantic from 2016 to 2021, Atmos. Chem. Phys., 22, 10919–10935, https://doi.org/10.5194/acp-22-10919-2022, 2022.

Terrenoire, E., Hauglustaine, D. A., Cohen, Y., Cozic, A., Valorso, R., Lefèvre, F., and Matthes, S.: Impact of present and future aircraft NO_x and aerosol emissions on atmospheric composition and associated direct radiative forcing of climate, Atmos. Chem. Phys., 22, 11987–12023, https://doi.org/10.5194/acp-22-11987-2022, 2022.

Tremmel, H. G., Schlager, H., Konopka, P., Schulte, P., Arnold, F., Klemm, M., and Droste-Franke, B.: Observations and model calculations of jet aircraft exhaust products at cruise altitude and inferred initial OH emissions, J. Geophys. Res.-Atmos., 103, 10803–10816, https://doi.org/10.1029/97JD03451, 1998.

Voigt, C., Jurkat, T., Schlager, H., Schäuble, D., Petzold, A., and Schumann, U.: Aircraft Emissions at Cruise and Plume Processes, in: Atmospheric Physics: Background – Methods – Trends, edited by: Schumann, U., Springer Berlin Heidelberg, Berlin, Heidelberg, 675–692, https://doi.org/10.1007/978-3-642-30183-4_41, 2012.

Voigt, C., Schumann, U., Jessberger, P., Jurkat, T., Petzold, A., Gayet, J.-F., Krämer, M., Thornberry, T., and Fahey, D. W.: Extinction and optical depth of contrails, Geophys. Res. Lett., 38, L11806, https://doi.org/10.1029/2011GL047189, 2011.

Voigt, C., Kleine, J., Sauer, D., Moore, R. H., Bräuer, T., Le Clercq, P., Kaufmann, S., Scheibe, M., Jurkat-Witschas, T., Aigner, M., Bauder, U., Boose, Y., Borrmann, S., Crosbie, E., Diskin, G. S., DiGangi, J., Hahn, V., Heckl, C., Huber, F., Nowak, J. B., Rapp, M., Rauch, B., Robinson, C., Schripp, T., Shook, M., Winstead, E., Ziemba, L., Schlager, H., and Anderson, B. E.: Cleaner burning aviation fuels can reduce contrail cloudiness, Commun. Earth Environ., 2, 114, https://doi.org/10.1038/s43247-021-00174-y, 2021.

Voigt, C., Lelieveld, J., Schlager, H., Schneider, J., Curtius, J., Meerkötter, R., Sauer, D., Bugliaro, L., Bohn, B., Crowley, J. N., Erbertseder, T., Groß, S., Hahn, V., Li, Q., Mertens, M., Pöhlker, M. L., Pozzer, A., Schumann, U., Tomsche, L., Williams, J., Zahn, A., Andreae, M., Borrmann, S., Bräuer, T., Dörich, R., Dörnbrack, A., Edtbauer, A., Ernle, L., Fischer, H., Giez, A., Granzin, M., Grewe, V., Harder, H., Heinritzi, M., Holanda, B. A., Jöckel, P., Kaiser, K., Krüger, O. O., Lucke, J., Marsing, A., Martin, A., Matthes, S., Pöhlker, C., Pöschl, U., Reifenberg, S., Ringsdorf, A., Scheibe, M., Tadic, I., Zauner-Wieczorek, M.,

Henke, R., and Rapp, M.: Cleaner Skies during the COVID-19 Lockdown, B. Am. Meteorol. Soc., 103, E1796–E1827, https://doi.org/10.1175/BAMS-D-21-0012.1, 2022.

Wormhoudt, J., Herndon, S. C., Yelvington, P. E., Miake-Lye, R. C., and Wey, C.: Nitrogen Oxide (NO/NO_2/HONO) Emissions Measurements in Aircraft Exhausts, J. Propul. Power, 23, 906–911, https://doi.org/10.2514/1.23461, 2007.

Yelugoti, S. R. and Wang, W.-C.: The combustion performance of sustainable aviation fuel with hydrogen addition, Int. J. Hydro. Energy, 48, 15, 130–6145, https://doi.org/10.1016/j.ijhydene.2022.11.104, 2023.

Ziereis, H., Schlager, H., Schulte, P., van Velthoven, P. F. J., and Slemr, F.: Distributions of NO, NO_x, and NO_y in the upper troposphere and lower stratosphere between 28° and 61° N during POLINAT 2, J. Geophys. Res.-Atmos., 105, 3653–3664, https://doi.org/10.1029/1999JD900870, 2000.

Ziereis, H., Hoor, P., Grooß, J.-U., Zahn, A., Stratmann, G., Stock, P., Lichtenstern, M., Krause, J., Bense, V., Afchine, A., Rolf, C., Woiwode, W., Braun, M., Ungermann, J., Marsing, A., Voigt, C., Engel, A., Sinnhuber, B.-M., and Oelhaf, H.: Redistribution of total reactive nitrogen in the lowermost Arctic stratosphere during the cold winter 2015/2016, Atmos. Chem. Phys., 22, 3631–3654, https://doi.org/10.5194/acp-22-3631-2022, 2022.